Наносистеми, наноматеріали, нанотехнології
Nanosistemi, Nanomateriali, Nanotehnologii
2026, т. 24, № 2, сс. 489–502
https://doi.org/10.15407/nnn.24.02.0489

PACS numbers: 68.35.Ct, 68.37.Ps, 68.47.Gh, 68.55.J-, 81.15.Cd, 81.16.Pr, 81.65.Mq

Influence of Cr^{3+} and Mn^{2+} Activators on the Surface Morphology Formation of $ZnGa_2O_4$ Thin Films Obtained by RF Ion-Plasma Sputtering

I. I. Medvid[1], I. Yo. Kukharskyy[1], I. O. Bordun[1], V. G. Bihday[1], Zh. Ya. Tsapovska[1], I. M. Kofliuk[1], D. S. Leonov[2], and O. M. Bordun[1]

[1]*Ivan Franko National University of Lviv,*
50, Drahomanov Str.,
UA-79005 Lviv, Ukraine
[2]*Technical Centre, N.A.S. of Ukraine,*
13, Pokrovska Str.,
UA-04070 Kyiv, Ukraine

The surface morphology of zinc gallate ($ZnGa_2O_4$) thin films doped with Mn^{2+} and Cr^{3+} ions, obtained by RF ion-plasma sputtering on fused quartz (υ-SiO_2) substrates, is analyzed. The influence of the activator type on the values of statistical surface-roughness parameters, grain sizes, and the nature of their distribution is investigated, using atomic force microscopy (AFM). As established, as-deposited $ZnGa_2O_4$:Mn films possess a fine-grained structure with pronounced nanopeaks (with coefficient of kurtosis $S_{ka} = 6.4$), whereas $ZnGa_2O_4$:Cr films are characterized by larger grains and higher root-mean-square (RMS) roughness. As shown, thermal treatment leads to an increase in the grain size of the investigated samples. The results are explained, based on the crystallochemical features of the substitution of Zn^{2+} and Ga^{3+} ions by Mn^{2+} and Cr^{3+} ions in the corresponding positions of the spinel crystal structure.

Проведено аналізу морфології поверхні тонких плівок ґалату Цинку ($ZnGa_2O_4$), леґованих йонами Mn^{2+} і Cr^{3+}, одержаних методом ВЧ-йонно-плазмового розпорошення на підкладинках із топленого кварцу υ-SiO_2. За допомогою атомно-силової мікроскопії (АСМ) досліджено вплив типу активатора на значення статистичних параметрів шерсткости поверхні, розміри зерен і характер їхнього розподілу. Встановлено, що невідпалені плівки $ZnGa_2O_4$:Mn мають дрібнозернисту структуру з вираженими нанопіками (коефіцієнт ексцесу — $S_{ka} = 6{,}4$), тоді як плівки $ZnGa_2O_4$:Cr характеризуються більшими зернами та вищою середньоквадратичною шерсткістю. Показано, що термічне оброблення приводить до збільшення розмірів зерен досліджуваних зразків. Результати пояснено на

основі кристалохемічних особливостей заміщення йонів Zn^{2+} і Ga^{3+} йонами Mn^{2+} і Cr^{3+} у відповідних позиціях кристалічної структури шпінелі.

Key words: zinc gallate, manganese activator, chromium activator, thin films, crystallites, surface morphology, AFM, thin-film annealing.

Ключові слова: ґалат Цинку, манґановий активатор, хромовий активатор, тонкі плівки, кристаліти, морфологія поверхні, АСМ, відпал тонких плівок.

(Received 19 May, 2026)

1. INTRODUCTION

Zinc gallate ($ZnGa_2O_4$) is a wide-band gap metal oxide semiconductor that attracts significant scientific interest among researchers due to its wide range of potential practical applications. At present, the properties of both undoped and doped $ZnGa_2O_4$ thin films obtained by various methods are being actively investigated. Zinc gallate is a representative of ternary materials with a band gap in the range from 4.4 to 5.2 eV and is characterized by good optical and electrical properties. In particular, $ZnGa_2O_4$ is a transparent conducting oxide in the ultraviolet and visible spectral regions and is also characterized by high chemical and thermal stability [1–3]. Due to the combination of its wide band gap, high stability, characteristic intrinsic blue emission, and efficient cathodoluminescent properties, $ZnGa_2O_4$ is considered a promising material for display systems and is used, in particular, in field emission displays (FED) [4]. The luminescent properties of $ZnGa_2O_4$ vary significantly depending on the stoichiometric composition of the material, the presence of dopants, as well as the surface properties of the thin films. In this context, Mn^{2+} and Cr^{3+} transition metal ions are effective luminescence activators of $ZnGa_2O_4$, providing green and red emission, respectively.

Among oxide materials, $ZnGa_2O_4$ demonstrates great promise for applications in optoelectronic devices, power electronics, gas sensors, and photodetectors, specifically deep-ultraviolet photodetectors (DUV PDs), solar-blind ultraviolet (UV) photodetectors, and x-ray photodetectors (XPDs), which can be utilized in medical imaging systems [5–11]. Moreover, $ZnGa_2O_4$ is used in photocatalysis and is a promising material for the fabrication of sensitive films in EGFET-type pH sensors [12]. Due to its electrical properties, $ZnGa_2O_4$ is also considered as a promising material for the fabrication of transistors, voltage converters, and high-efficiency Schottky diodes [13].

The physical properties of zinc gallate thin films depend not only on the type and on concentration of dopants, but on the deposition method and post-deposition treatment techniques too. In general, the properties of polycrystalline thin films are significantly determined by the surface morphology, in particular by the crystallite sizes, as well as by the energy levels arising from the presence of grain boundaries. The situation is complicated by the fact that the film structure is often far from perfect, which necessitates a detailed investigation of their surface morphology.

In this regard, the present work analyzed the influence of Mn^{2+} and Cr^{3+} activators on the surface morphology of $ZnGa_2O_4$ thin films. The study was conducted using atomic force microscopy (AFM), which allows not only for the visualization of surface topography, but also for the quantitative assessment of surface parameters that directly affect the performance characteristics of semiconductor devices. Thin-film samples were obtained by RF ion-plasma sputtering, which ensures the formation of homogeneous semiconductor and dielectric films [14].

2. EXPERIMENTAL TECHNIQUE

The deposition of $ZnGa_2O_4$:Mn and $ZnGa_2O_4$:Cr thin films with a thickness of 0.3–1.0 μm was performed in an argon atmosphere using RF ion-plasma sputtering. Fused quartz of amorphous structure υ-SiO_2 was used as substrates for thin film deposition. RF sputtering was carried out in a system using the magnetic field of external solenoids for compression and additional ionization of the plasma column. The starting material consisted of a stoichiometric mixture of high-purity ZnO and Ga_2O_3 oxides. The Mn and Cr activator concentration amounted to 1 mol.%. Post-deposition thermal treatment of the films on amorphous υ-SiO_2 substrates was carried out in an air atmosphere at 1000–1100°C. Before film sputtering, the substrates were subjected to chemical cleaning and thermal annealing cycles to eliminate surface impurities and residual thermal stresses.

The phase composition and structure of the obtained thin films were investigated by x-ray diffraction analysis (Shimadzu XRD-600). The x-ray structural studies described previously revealed a polycrystalline structure for the obtained films [15]. The elemental analysis of the samples was performed at several points on the thin film surface using an OXFORD INCA Energy 350 energy-dispersive spectrometer. The elemental composition analysis of the surface of the obtained thin-film samples was performed by x-ray photoelectron spectroscopy (XPS). XPS spectra (Phoibos 150, Specs) were recorded using a monochromatic AlK_α x-ray source (1486.6 eV). The binding energy was calibrated using the C1*s* signal at 285.0 eV.

Atomic force microscopy (AFM, INTEGRA TS-150) was employed to study the surface morphology of the thin films. Surface images of the thin films were recorded in tapping mode using NSG10 series silicon cantilevers with a resonant frequency of 323 kHz and a force constant of 24 N/m. Processing of the obtained experimental data and calculation of surface morphology parameters were performed using Image Analysis 3.5 software.

3. RESULTS AND DISCUSSION

Two-dimensional (2*D*) and three-dimensional (3*D*) AFM images of the surfaces of as-deposited $ZnGa_2O_4$:Cr and $ZnGa_2O_4$:Mn thin films obtained by RF ion plasma sputtering on fused quartz (υ-SiO_2) substrates are shown in Fig. 1.

A series of standard surface parameters, including root mean square roughness (RMS), average roughness, mean grain diameter, mean grain area and volume, grain height with maximum grain count, coefficient of kurtosis, peak-to-peak, and surface skewness, were determined from AFM images of $ZnGa_2O_4$:Cr and $ZnGa_2O_4$:Mn

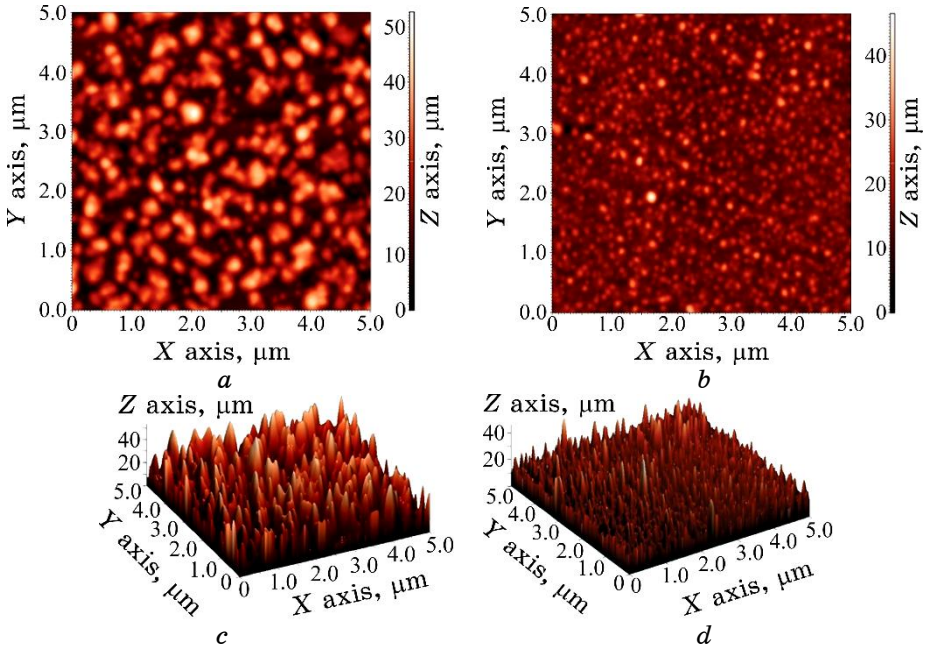

Fig. 1. Surface morphology images of as-deposited (*a*, *c*) $ZnGa_2O_4$:Cr and (*b*, *d*) $ZnGa_2O_4$:Mn thin films obtained by RF sputtering on υ-SiO_2 substrates. Images (*a*) and (*b*) are 2*D*, while (*c*) and (*d*) are 3*D*.

TABLE 1. Surface morphology parameters of as-deposited $ZnGa_2O_4$:Mn and $ZnGa_2O_4$:Cr thin films.

Parameter	$ZnGa_2O_4$:Mn	$ZnGa_2O_4$:Cr
Root-mean-square roughness, S_q, nm	3,9	9,6
Average roughness, S_a, nm	2.9	8.1
Mean grain diameter, D, nm	113	211
Mean grain area, S, nm^2	4730	12100
Mean grain volume, V, nm^3	11400	67600
Grain height with maximum grain count, h, nm	13	11
Coefficient of kurtosis, S_{ka}	6.4	2.3
Peak-to-peak, S_y, nm	46.5	53.5
Surface skewness, S_{sk}	1.5	0.5

thin films over a 5000×5000 nm scan area. Characteristic parameters calculated using the Image Analysis 3.5 software for as-deposited $ZnGa_2O_4$:Mn and $ZnGa_2O_4$:Cr thin films obtained by RF sputtering on υ-SiO_2 substrates are summarized in Table 1.

As seen from the presented results, the dopant type has a significant influence on the crystalline grain size and surface roughness of the activated $ZnGa_2O_4$ thin films obtained by RF sputtering on υ-SiO_2 substrates. Analysis of the AFM images (Fig. 1) of as-deposited $ZnGa_2O_4$:Cr and $ZnGa_2O_4$:Mn thin films shows that the films doped with Cr^{3+} ions are characterized by a coarser homogeneous structure with well-defined large grains. In contrast, the films doped with Mn^{2+} ions exhibit a fine-grained surface morphology with thinner needle-like grains on the surface. This is confirmed by the obtained parameters of the crystalline grains on the surface of the investigated $ZnGa_2O_4$:Mn and $ZnGa_2O_4$:Cr thin films (Table 1), as the grain sizes of the $ZnGa_2O_4$:Cr films are significantly larger compared to the crystallite sizes of the $ZnGa_2O_4$:Mn thin films. For instance, the mean grain diameter of the $ZnGa_2O_4$:Cr thin films is of 211 nm, whereas, for the $ZnGa_2O_4$:Mn films, it is of 113 nm, which is almost twice as small as the mean diameter for the $ZnGa_2O_4$:Cr thin films.

In Ref. [16], it is noted that $ZnGa_2O_4$ can be considered as a complex oxide consisting of ZnO and Ga_2O_3, with a spinel structure of the general chemical formula AB_2O_4, where Zn^{2+} ions occupy tetrahedral sites and Ga^{3+} ions occupy octahedral sites. The authors of that study note that while it is difficult for Mn^{2+} ions to substitute for Ga^{3+} ions, they easily replace Zn^{2+} ions. The analysis was conducted based on the calculation of the effective compensation coefficient for ion substitution, φ, the value of which was calculated using the formula: $\varphi = Z/r$, where Z is the ion charge and r is its effective radius [16]. The same study [16] also states that in

$ZnGa_2O_4$, ions with similar effective radii substitute for each other more easily; that is, Cr^{3+} more readily replaces Ga^{3+}, while Mn^{2+} more easily substitutes for Zn^{2+}. It should also be taken into account that the coordination number of the Zn^{2+} cation in the tetrahedral position is 4, while that of Ga^{3+} in the octahedral position is 6 [17–19]. In Ref. [20], it is stated that the ionic radii of Cr^{3+} and Ga^{3+} in octahedral coordination are nearly identical and are approximately 0.62 Å. This makes the $ZnGa_2O_4$ host matrix ideal for the incorporation of Cr^{3+} ions without significant changes or stresses in the crystal lattice structure. Since the charges of Zn^{2+} and Mn^{2+} ions are identical (isovalent substitution occurs), the $ZnGa_2O_4$ structure does not require additional charge compensation. This facilitates the effective substitution of Zn^{2+} ions, which have a smaller ionic radius (0.60 Å), by Mn^{2+} ions with a slightly larger ionic radius (0.66 Å) in the tetrahedral sites of the crystal lattice [21].

The data in Table 1, obtained from the AFM images of as-deposited $ZnGa_2O_4$:Mn thin films (Fig. 1), indicate the formation of a fine-grained morphology. This is most likely due to the occurrence of local microstresses in the crystal lattice caused by the difference in the ionic radii of Mn^{2+} and Zn^{2+}, which limits crystallite growth during the film deposition process. For the as-deposited $ZnGa_2O_4$:Cr thin films, the Cr impurity predominantly substitutes for Ga, forming a rougher surface with root-mean-square roughness (S_q) of 9.6 nm and average roughness (S_a) of 8.1 nm, which are approximately 2.5 and 2.8 times higher than the corresponding values for the as-deposited $ZnGa_2O_4$:Mn thin films. Since the ionic radii of Cr^{3+} and Ga^{3+} in octahedral coordination are nearly identical, the substitution occurs without significant structural distortions. This facilitates active grain growth and the formation of a well-developed surface microrelief.

A statistical analysis of the surface roughness heights (the grains that form the sample morphology) indicates that for a normal (Gaussian) distribution, the S_q/S_a ratio equals 1.25 [22, 23]. As also noted in Ref. [23], the height distribution of surface irregularities for most engineering surfaces can be approximately described by a normal (Gaussian) distribution with S_q/S_a ratio values up to 1.31. Analysis of the obtained results showed that for the as-deposited $ZnGa_2O_4$:Mn film, the S_q/S_a ratio is of 1.34, which exceeds the value of 1.31. This indicates that the distribution does not follow a normal pattern and points to a complex relief dominated by high nanopeaks (Fig. 1). Analysis of the grains' height distribution histograms (Fig. 2) shows that for the as-deposited $ZnGa_2O_4$:Mn thin films, a long 'tail' is observed toward larger height values, indicating the presence of extreme peaks ('needles') on the sample surface. For the as-deposited $ZnGa_2O_4$:Cr thin films obtained by RF sputter-

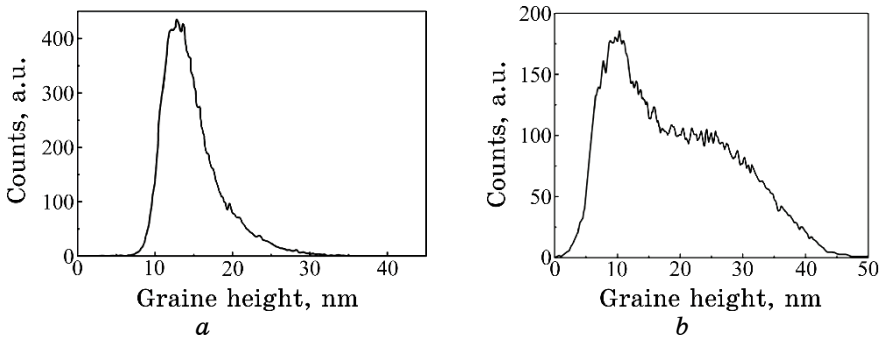

Fig. 2. Grain height distribution on AFM images of as-deposited (*a*) $ZnGa_2O_4$:Mn and (*b*) $ZnGa_2O_4$:Cr thin films obtained by RF sputtering on υ-SiO_2 substrates.

ing on υ-SiO_2 substrates, the S_q/S_a ratio is of 1.18. This value is lower than the optimal value of 1.25 for a normal distribution, indicating the formation of a more homogeneous structure and the absence of random peaks. The height histogram for the as-deposited $ZnGa_2O_4$:Cr thin films is characterized by a broad distribution of grain heights with more complex shapes (Fig. 2).

For a more detailed assessment of the influence of dopant type on the surface topology of the thin films, we analyze the values of the surface skewness, S_{sk}, and the coefficient of kurtosis, S_{ka}. In studies [23, 24], it is noted that the surface skewness parameter is sensitive to isolated deep valleys or high peaks; accordingly, a symmetric grain height distribution, which has an equal number of valleys and peaks and corresponds to a normal distribution, has zero skewness. Surfaces with the presence of high peaks exhibit positive skewness. This parameter indicates the direction in which the height distribution is shifted relative to the mean line [24]. For the as-deposited $ZnGa_2O_4$:Mn and $ZnGa_2O_4$:Cr thin films obtained by RF sputtering on υ-SiO_2 substrates, the S_{sk} values are 1.5 and 0.5, respectively. The surface skewness values for both samples are positive ($S_{sk} > 0$), indicating that the surface of both films is composed predominantly of peaks (hills), *i.e.*, crystallites protruding above the valleys. This is more clearly observed for $ZnGa_2O_4$:Mn thin films, where the surface morphology is determined by the presence of high nanostructures on the background layer, forming a needle-like structure. In contrast, $ZnGa_2O_4$:Cr thin films exhibit a smoother, more homogeneous relief composed of larger grains.

To describe the distribution of sharp peaks above and below the mean line when characterizing surface morphology images, the coefficient of kurtosis parameter, S_{ka}, is used. In studies [23–25], it is noted that at a value of $S_{ka} < 3$, the surface is characterized by a

smoothed structure, meaning the surface is formed by a large number of grains of average height with a relatively small number of high peaks and deep valleys; such a distribution is termed platykurtic. If $S_{ka} > 3$, the surface is characterized by a relatively large number of pronounced peaks, *i.e.*, a 'spiky' shape, and the grain height distribution is referred to as leptokurtic. A value of $S_{ka} = 3$ corresponds to an ideal normal (Gaussian) grain height distribution [26]. The kurtosis coefficient values are in good agreement with the above-analyzed characteristics and amount to 6.4 and 2.3 for the surfaces of $ZnGa_2O_4$:Mn and $ZnGa_2O_4$:Cr thin films, respectively. For the $ZnGa_2O_4$:Cr films, $S_{ka} < 3$ that indicates a smoother structure; that is, the film surface is formed by relatively gentle and rounded grain tops without the presence of local sharp peaks. The S_{ka} value for the as-deposited $ZnGa_2O_4$:Mn thin films differs significantly from the corresponding value for the as-deposited $ZnGa_2O_4$:Cr thin films, indicating the influence of the dopant type on the formation of surface morphology. The S_{ka} parameter value for as-deposited $ZnGa_2O_4$:Mn thin films is of 6.4, which is significantly greater than 3. This indicates the presence of sharp and narrow peaks on the surface and corresponds to a leptokurtic distribution. According to Refs. [24, 25], the surface profile skewness S_{sk} and the kurtosis coefficient S_{ka} for a surface profile with N points (grains) are calculated using the following formulas:

$$S_{sk} = \frac{1}{NS_q^3} \sum_{i=1}^{N} y_i^3 , \tag{1}$$

$$S_{ka} = \frac{1}{NS_q^4} \sum_{i=1}^{N} y_i^4 , \tag{2}$$

where S_q is the root mean square (RMS) surface roughness and y_i is the height of the profile (grains) at point i relative to the mean line.

For the analysis of thin film surface morphology, statistical parameters such as grain count and grain size distribution (for instance, distribution by grain diameter, area, or volume) are also used. Grain count analysis of the surfaces of as-deposited $ZnGa_2O_4$:Mn and $ZnGa_2O_4$:Cr thin films, obtained by RF sputtering on υ-SiO_2 substrates, revealed that Mn^{2+}-activated films contain nearly 3.4 times more grains per unit area compared to Cr^{3+}-activated films. In addition to the dopant type, the molar concentration of the dopant can also influence the formation of the surface morphology. In study [27], SEM micrograph analysis shows that the molar concentration of Cr^{3+} ions influences the morphology of $ZnGa_2O_4$ nanopowders. An AFM study of the influence of dopant concentration on the surface morphology of thin oxide films was

conducted in Ref. [28].

Investigations of thin oxide film surface morphology, specifically $ZnGa_2O_4$, demonstrate that thermal treatment of the studied samples results in modifications of the film surfaces. Important factors in this process are both the temperature and the atmosphere in which the thermal treatment of the films is carried out, since they can differently influence the formation of thin film surface morphology. A detailed analysis of the influence of the annealing atmosphere on the surface morphology and XPS spectra of $ZnGa_2O_4$:Mn and $ZnGa_2O_4$:Cr thin films was carried out in Refs. [29] and [30], respectively. The obtained results showed that the presence of thermal treatment has a significant effect on the size of crystalline grains and the surface roughness of the films. It should be noted that a similar situation is observed during RF sputtering on amorphous υ-SiO_2 substrates and for thin films based on β-Ga_2O_3 [31, 32], where it is reported that thermal treatment leads to grain growth due to processes of growth and sintering. In study [33], the effect of annealing temperature on the surface morphology of $ZnGa_2O_4$ films was investigated, and it was shown that at high temperatures annealing of thin films leads to the appearance of an additional Ga_2O_3 phase alongside the existing $ZnGa_2O_4$ phase, since Zn atoms diffuse out of the film surface during high-temperature annealing. Investigations conducted in Ref. [34] demonstrated that the surface morphology of $ZnGa_2O_4$ thin films is also influenced by the sample preparation technique.

For the analysis of surface morphology, the parameter of peak-to-peak, S_y, is used. It characterizes the maximum height of the profile or surface and is defined as the vertical distance between the highest point (peak) and the lowest point (valley) within the scanning area [25, 35]. For the as-deposited $ZnGa_2O_4$:Cr and $ZnGa_2O_4$:Mn thin films obtained by RF ion-plasma sputtering on amorphous fused quartz (υ-SiO_2) substrates, the S_y values are 53.5 nm and 46.5 nm, respectively. This confirms that the $ZnGa_2O_4$:Cr thin films are formed from flatter grains of a larger size, whereas the surface of the $ZnGa_2O_4$:Mn thin films exhibits higher peaks (grains).

It is interesting to compare the obtained results with the results of the study of the surface morphology of $ZnGa_2O_4$:Cr and $ZnGa_2O_4$:Mn thin films obtained by RF ion-plasma sputtering on fused quartz (υ-SiO_2) substrates and annealed in air atmosphere. Two-dimensional (2*D*) and three-dimensional (3*D*) AFM micrographs of the surface morphology of $ZnGa_2O_4$:Cr and $ZnGa_2O_4$:Mn films after thermal treatment in air atmosphere are shown in Fig. 3.

The statistical standard parameters calculated on the basis of AFM images of the surface morphology of $ZnGa_2O_4$:Mn and $ZnGa_2O_4$:Cr thin films after thermal treatment in air atmosphere for

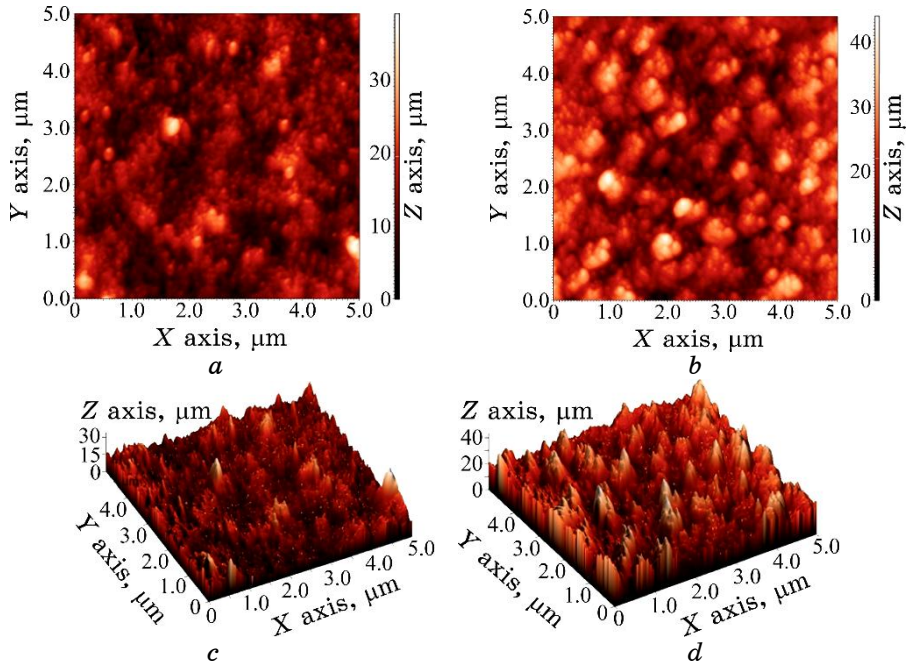

Fig. 3. Surface morphology images of (*a*, *c*) $ZnGa_2O_4$:Cr and (*b*, *d*) $ZnGa_2O_4$:Mn thin films obtained by RF sputtering on υ-SiO_2 substrates after thermal treatment in air atmosphere. Images *a* and *b* are two-dimensional, while *c* and *d* are three-dimensional.

areas of identical size (5000×5000 nm) are presented in Table 2.

Investigations on the influence of the annealing atmosphere on the formation of the surface morphology of $ZnGa_2O_4$:Cr and

TABLE 2. Surface morphology parameters of $ZnGa_2O_4$:Mn and $ZnGa_2O_4$:Cr thin films after thermal treatment in air atmosphere.

Parameter	$ZnGa_2O_4$:Mn	$ZnGa_2O_4$:Cr
Average roughness, S_a, nm	5.0	3.4
Root-mean-square roughness, S_q, nm	6.2	4.4
Mean grain diameter, D, nm	274	316
Mean grain area, S, nm^2	23900	30400
Mean grain volume, V, nm^3	65700	115000
Grain height with maximum grain count, h, nm	18	12
Coefficient of kurtosis, S_{ka}	2.97	5.0
Peak-to-peak, S_y, nm	43.9	38.9
Surface skewness, S_{sk}	0.4	0.9

$ZnGa_2O_4$:Mn thin films, conducted in Refs. [29, 30], showed that annealing stimulates grain boundary migration and promotes the coalescence of some grains during the thermal treatment process of the thin films. At high annealing temperatures, Zn atoms diffuse from the film surface [31], while grains with lower surface energy grow through the grain growth process. However, for the investigated samples, annealing in air atmosphere affects the formation of the surface morphology differently, which may be related to the fact that Mn^{2+} ions substitute Zn^{2+} ions, whereas Cr^{3+} ions more easily replace Ga^{3+} ions. $ZnGa_2O_4$:Mn thin films after annealing in air atmosphere are characterized by an almost ideal normal distribution of grain heights, since the S_{ka} value is of 2.97 and the S_q/S_a ratio is of 1.24, which indicates the relaxation of sharp peaks typical for the as-deposited films. The set of values of the parameters S_q, S_a, D, S, V, and S_y confirms significant uniform grain growth perpendicular to the film surface. For the annealed $ZnGa_2O_4$:Cr thin films, the D, S and V values are significantly larger than those for the annealed $ZnGa_2O_4$:Mn films are; however, the S_q, S_a and S_y values are smaller, which indicates planar grain growth, *i.e.*, parallel to the film surface. The large S_{ka} value indicates the presence of individual dominant peaks on the surface of the annealed $ZnGa_2O_4$:Cr thin films. For the annealed $ZnGa_2O_4$:Cr and $ZnGa_2O_4$:Mn films, the S_{sk} value is positive, which indicates that the surface of both films is formed by predominant peaks (hills) rather than valleys. Mn^{2+} and Cr^{3+} ions, substituting for Zn^{2+} and Ga^{3+} ions in the tetrahedral and octahedral sites of the $ZnGa_2O_4$ structure, respectively, exert different influences on the processes of nucleation, grain growth, and diffusion during high-temperature annealing. This leads to significant differences in the surface morphology of the thin films both before and after thermal treatment at 1000°C in air atmosphere.

4. CONCLUSIONS

It was established that RF ion-plasma sputtering on amorphous υ-SiO_2 substrates yields $ZnGa_2O_4$:Cr and $ZnGa_2O_4$:Mn thin films formed of nanometer-sized grains. The influence of the activator type, Mn^{2+} and Cr^{3+}, on the formation of the surface morphology of as-deposited and annealed $ZnGa_2O_4$:Cr and $ZnGa_2O_4$:Mn thin films in air atmosphere at 1000°C has been analyzed. As established, the activator type significantly affects the growth behaviour of the films. The as-deposited $ZnGa_2O_4$:Cr thin films are characterized by a coarse-grained structure with a large mean grain diameter of 211 nm and a root-mean-square surface roughness of 9.6 nm. During growth, the $ZnGa_2O_4$:Mn thin films are formed of grains with an average diameter of 113 nm and a root-mean-square surface rough-

ness of 3.9 nm, exhibiting a surface with a large number of sharp nanopeaks. Analysis of the surface skewness and coefficient of kurtosis parameters showed that the as-deposited $ZnGa_2O_4$:Mn thin films are characterized by a leptokurtic distribution of grain heights, whereas the surface of the $ZnGa_2O_4$:Cr films is smoother and exhibits a platykurtic distribution. It is proposed that the substantial differences in the surface morphology of $ZnGa_2O_4$:Mn and $ZnGa_2O_4$:Cr thin films, both before and after thermal treatment at 1000°C in air atmosphere, are due to the fact that the Mn^{2+} and Cr^{3+} activator ions occupy the oxygen-coordinated tetrahedral and octahedral sites of the Zn^{2+} and Ga^{3+} ions, respectively, in the $ZnGa_2O_4$ spinel structure; consequently, they differently affect crystal lattice distortion, nucleation, grain growth and sintering processes, as well as Zn^{2+} ion diffusion during high-temperature annealing.

REFERENCES

1. Yan Jin-Liang, Zhao Yin-Nü, and Li Chao, *Chin. Phys. B*, **23**, No. 4: 048105 (2014); https://doi.org/10.1088/1674-1056/23/4/048105
2. Wei-Kai Wang, Kuo-Feng Liu, Sung-Yu Wang, Jian-Cheng Guo, and Shih-Yung Huang, *Semicond. Sci. Technol.*, **36**: 055011 (2021); https://doi.org/10.1088/1361-6641/abefa2
3. Samiran Bairagi, Ching-Lien Hsiao, Roger Magnusson, Jens Birch, Jinn P. Chu, Fu-Gow Tarntair, Ray-Hua Horng, and Kenneth Järrendahl, *Optical Materials Express.*, **12**, No. 8: 3284 (2022); https://doi.org/10.1364/OME.462668
4. Su-Hua Yang, Chien-Yuan Lu, and Shoou-Jinn Chang, *Journal of The Electrochemical Society*, **154**, No. 8: J229 (2007); https://doi.org/10.1149/1.2740027
5. Jia-Hang Liu, Lei Li, Fan Zhang, Ya-Ping Qi, Zhen-Ping Wu, and Wei-Hua Tang, *Phys. Scr.*, **99**: 055538 (2024); https://doi.org/10.1088/1402-4896/ad3b4f
6. L.-C. Cheng, C.-Y. Huang, and R.-H. Horng, *Journal of the Electron Devices Society*, **6**: 432 (2018); https://doi.org/10.1109/JEDS.2018.2803078
7. Chengling Lu, Qingyi Zhang, Shan Li, Zuyong Yan, Zeng Liu, Peigang Li and Weihua Tang, *J. Phys. D: Appl. Phys.*, **54**: 405107 (2021); https://doi.org/10.1088/1361-6463/ac1465
8. Anqi Guo, Lichun Zhang, Ning Cao, Taiping Lu, Yadan Zhu, Dan Tian, Zhiying Zhou, Shunli He, Bin Xia, and Fengzhou Zhao, *Appl. Phys. Express*, **16**, No. 2: 021004 (2023); https://doi.org/10.35848/1882-0786/acb98c
9. Ray-Hua Horng, Peng-Hsuan Huang, Yun-Sheng Li, Fu-Gow Tarntair, and Chih Shan Tan, *Appl. Surf. Sci.*, **555**: 149657 (2021); https://doi.org/10.1016/j.apsusc.2021.149657
10. Wanmin Lin, Dan Zhang, Sixian Liu, Yuqiang Li, Wei Zheng, and Feng Huang, *Mater. Lett.*, **283**: 128805 (2021); https://doi.org/10.1016/j.matlet.2020.128805
11. Anoop Kumar Singh, Shiau-Yuan Huang, Po-Wei Chen, Jung-Lung Chiang,

and Dong-Sing Wuu, *Nanomaterials*, **11**: 2316 (2021); https://doi.org/10.3390/nano11092316
12. Chia-Hsun Chen, Shu-Bai Liu, and Sheng-Po Chang, *ACS Omega*, **9**, Iss. 13: 15304 (2024); https://doi.org/10.1021/acsomega.3c09965
13. Yi-Siang Shen, Wei-Kai Wang, and Ray-Hua Horng, *Journal of the Electron Devices Society*, **5**, Iss. 2: 112 (2017); doi:10.1109/JEDS.2017.2653419
14. Kiyotaka Wasa, Makoto Kitabatake, and Hideaki Adachi, *Thin Film Materials Technology: Sputtering of Compound Materials* (New York: William Andrew Inc. publishing–Springer-Verlag GmbH&Co. KG: 2004).
15. O. M. Bordun, I. Yo. Kukharskyy, and V. G. Bihday, *J. Appl. Spectrosc.*, **78**, No. 6: 922 (2012); https://doi.org/10.1007/s10812-012-9555-9
16. Yan Liu, Tingting Zheng, Xiuyun Zhang, and Chen Chen, *Scientific Reports*, **13**: 14430 (2023); https://doi.org/10.1038/s41598-023-41658-5
17. Shigeaki Ono, John P. Brodholt, and G. David Price, *Phys. Chem. Miner.*, **35**: 381 (2008); https://doi.org/10.1007/s00269-008-0231-9
18. D. Errandonea, Ravhi S. Kumar, F. J. Manjyn, V. V. Ursaki, and E. V. Rusu, *Phys. Rev. B*, **79**: 024103 (2009); https://doi.org/10.1103/PhysRevB.79.024103
19. O. M. Bordun, I. I. Medvid, I. Y. Kukharskyy, M. V. Protsak, I. O. Bordun, I. M. Kofliuk, and K. L. Biliak, *Molecular Crystals and Liquid Crystals*, **769**, Nos. 7–8: 801 (2025); https://doi.org/10.1080/15421406.2025.2504059
20. Aurélie Bessière, Sylvaine Jacquart, Kaustubh Priolkar, Aurélie Lecointre, Bruno Viana, and Didier Gourier, *Optics Express.*, **19**, Iss. 11: 10132 (2011); https://doi.org/10.1364/OE.19.010131
21. K. Somasundaram, K. P. Abhilash, V. Sudarsan, P. Christopher Selvin, and R. M. Kadam, *Physica B*, **491**: 79 (2016); http://dx.doi.org/10.1016/j.physb.2016.03.022
22. Pawel Pawlus, Rafal Reizer, and Wieslaw Zelasko, *Materials*, **16**, No. 22: 7109 (2023); https://doi.org/10.3390/ma16227109
23. B. Rajesh Kumar and T. Subba Rao, *Digest Journal of Nanomaterials and Biostructures*, **7**, No. 4: 1881 (2012); https://www.researchgate.net/publication/279702126_AFM_studies_on_surface_morphology_topography_and_texture_of_nanostructured_zinc_aluminum_oxide_thin_films
24. E. S. Gadelmawla, M. M. Koura, T. M. A. Maksoud, I. M. Elewa, and H. H. Soliman, *Journal of Materials Processing Technology*, **123**, Iss. 1: 133 (2002); https://doi.org/10.1016/S0924-0136(02)00060-2
25. James Egbu, Paul R. Ohodnicki, Jr., John P. Baltrus, Ahmed Talaat, Ruishu F. Wright, and Michael E. McHenry, *Journal of Alloys and Compounds*, **912**: 165155 (2022); https://doi.org/10.1016/j.jallcom.2022.165155
26. B. Rajesh Kumar, B. Hymavathi, and T. Subba Rao, *Materials Today: Proceedings*, **4**: 8638 (2017); https://doi.org/10.1016/j.matpr.2017.07.212
27. M. K. Hussen and F. B. Dejene., *Optik.*, **181**: 514 (2019); https://doi.org/10.1016/j.ijleo.2018.12.121
28. O. M. Bordun, I. O. Bordun, I. M. Kofliuk, I. Yo. Kukharskyy, I. I. Medvid, Zh. Ya. Tsapovska, and D. S. Leonov, *Nanosistemi, Nanomateriali, Nanotehnologii*, **20**, Iss. 1: 91 (2022); https://doi.org/10.15407/nnn.20.01.91
29. O. M. Bordun, I. I. Medvid, I. Yo. Kukharskyy, I. O. Bordun,

M. V. Protsak, V. G. Bihday, I. S. Kuz, A. I. Tyslyuk, R. V. Pavlius, and D. S. Leonov, *Nanosistemi, Nanomateriali, Nanotehnologii*, **22**, Iss. 4: 823 (2024); https://doi.org/10.15407/nnn.22.04.823

30. O. M. Bordun, I. O. Bordun, I. I. Medvid, M. V. Protsak, I. Yo. Kukharskyy, V. G. Bihday, I. M. Kofliuk, I. Yu. Khomyshyn, and D. S. Leonov, *Nanosistemi, Nanomateriali, Nanotehnologii*, **21**, Iss. 4: 709 (2023); https://doi.org/10.15407/nnn.21.04.709
31. O. M. Bordun, B. O. Bordun, I. Yo. Kukharskyy, I. I. Medvid, I. I. Polovynko, Zh. Ya. Tsapovska, and D. S. Leonov, *Nanosistemi, Nanomateriali, Nanotehnologii*, **19**, Iss. 1: 159 (2021); https://doi.org/10.15407/nnn.19.01.159
32. O. M. Bordun, B. O. Bordun, I. I. Medvid, M. V. Protsak, I. Yo. Kukharskyy, K. L. Biliak, D. M. Maksymchuk, I. M. Kofliuk, and D. S. Leonov, *Nanosistemi, Nanomateriali, Nanotehnologii*, **22**, No. 1: 1 (2024); https://doi.org/10.15407/nnn.22.01.001
33. Wei-Kai Wang, Kuo-Feng Liu, Pi-Chuen Tsai, Yi-Jie Xu, and Shih-Yung Huang, *Coatings*, **9**, Iss. 12: 859 (2019); https://doi.org/10.3390/coatings9120859
34. O. M. Bordun, V. G. Bihday, I. Yo. Kukharskyy, I. I. Medvid, I. M. Kofliuk, I. Yu. Khomyshyn, Zh. Ya. Tsapovska, and D. S. Leonov, *Nanosistemi, Nanomateriali, Nanotehnologii*, **21**, Iss. 2: 403 (2023); https://doi.org/10.15407/nnn.21.02.403
35. G. Perfetti, T. Alphazana, P. van Hee, W. J. Wildeboer, and G. M. H. Meesters, *European Journal of Pharmaceutical Sciences*, **42**, Iss. 3: 262 (2011); https://doi.org/10.1016/j.ejps.2010.12.001